Novel Regenerative Braking Technique using BLDC Motors and Variable Stator Voltage for Enhanced EV Mileage: A Simulation Study

Vijay Pal[1], Pramod Kumar Rathore[2]

[1]M Tech Scholar, RKDF College of Engineering, Bhopal, Madhya Pradesh, India
[2]Assistant Professor, RKDF College of Engineering, Bhopal, Madhya Pradesh, India

ABSTRACT

Based on a Brushless DC (BLDC) motor, this research provides a novel regenerative braking approach. The recommended approach for braking involves using a variable Stator voltage from a multi-cell battery system DC-DC buck converter. To evaluate the performance of the proposed braking system, a simulation was used. According to simulation results, the proposed regenerative braking technique is practical and efficient. Additionally, this research introduces the most fundamental technology for regenerative braking using a BLDC motor to improve the mileage of lightweight electric vehicles (EVs).

KEYWORDS: Solar PV, Electric Vehicle, Regenerative Braking, Zeta Converter, P&O - MPPT, Battery & PMBLDC

I. INTRODUCTION

The major environmental hazards related with carbon emissions and the divestment of fossil fuels need the development of alternative or renewable energy sources. The shift from internal combustion engines to electric cars is a significant step forward for mankind towards the goal of zero carbon emissions and sustainable development. Due of its easier control algorithm than other EV motors, the PMBLDC motor has found broad application in light electric vehicle sectors such as e-rickshaws and two-wheelers. During deacceleration, energy is readily recovered in a PMBLDC motor and stored in the battery.

Electrical braking is often ineffective at speeds below a certain threshold, and energy cannot be recovered during emergency braking. Electronic and mechanical brake compatibility [1]. As illustrated in [2,] the amount of regeneration possible is dependent by the amount of braking pressure applied to the throttle. [3] features a fuzzy logic-based control system that improves braking performance substantially. Since sliding mode control provides excellent steady-state performance, it minimises unwanted oscillations in the DC bus while switching between driving and braking modes [4]. [5] use a bidirectional DC-DC converter to maintain DC bus voltage and reverse power flow when braking. The back emf of the motor must stay constant for effective battery charge [6].

To identify rotor position, find the zero-crossings of the rear emf [7]. The rotor position is also more precisely estimated by analysing the inverter switching function [8]. The third harmonic stator voltage waveform gives rotor position information and may be used to develop sensor-free approach.

The zeta converter is used to extract the greatest power from the solar panel while also offering consistent dynamic performance under a variety of environmental conditions. In solar-PV-based applications, the Zeta converter offers the following

specific advantages over conventional DC-DC converters:

➢ It can manage a wide range of MPPTs under dynamic settings since it operates in buck-boost mode. [12]. The highest duty ratio of a basic buck or boost converter refers to a certain mode of operation.

➢ The output inductor of the zeta converter ensures that there is no ripple current at the output of the boost or buck-boost converter [13].

➢ The zeta converter has noninverted output polarity, as opposed to the Cuk converter, which has both input and output ripple free current. As a consequence, negative voltage sensing is no longer required, reducing the complexity of sensor circuits. [14].

The solar-PV array and battery-powered PMBLDC motor drive are shown in Figure 1. A bidirectional DC-DC converter is used to link the battery to the DC connector, which increases the cost and weight. The bidirectional DC-DC converter regulates battery charging and discharging by maintaining the DC connection voltage. A DC-DC power converter is used at the front end of MPPT. Two voltage sensors, two current sensors, and hall sensors for position feedback are required for speed control. The dc-dc converter in [15] is replaced with a Z-source DC-DC converter. Controlling this kind of DC-DC converter, on the other hand, requires some complex control, such as monitoring phase currents and dc link voltage.

The following is an outline of the paper. Part II describes the system. Part III describes the design methods. Section IV covers the control methods used, followed by Section V's results and Section VI's conclusion.
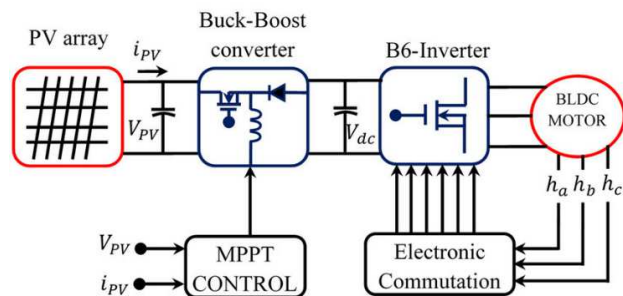
Fig 1: PV-powered BLDC motor driving system block diagram

II. SYSTEM DESCRIPTION AND OPERATION

A solar panel, a zeta converter, a three-phase voltage source inverter (VSI), and a PMBLDC motor comprise the vehicle's powertrain. Since the battery is connected to the system DC bus, the suggested

method eliminates the need for a second power converter and considerably reduces the number of sensors used. Just two voltage sensors are required in the proposed system to provide MPPT and sensor less control.

The engine needs electricity, which is provided by both the battery and the solar-PV panel. The maximum power collected by the solar panel is transferred to the VSI using a zeta converter. An incremental conductance approach is used for MPPT operation. The VSI and the intermediating zeta converter provide the whole electrical power from the DC bus to the load. The P&O-MPPT method is used by a pulse generator to create switching pulses for the zeta converter, which changes the duty ratio to operate the converter at maximum power. The estimated duty ratio is then compared to a high frequency carrier signal to guarantee maximum switching efficiency at the highest ideal power point for the converter. The electrical commutation logic of the PMBLDC motor controls the switching of the VSI's IGBTs. Since the VSI is switched at the fundamental frequency, switching losses are decreased. Additionally, energy is recycled bidirectionally from both sources to loads. The VSI is now charging the battery and serving as a rectifier. It is also feasible to implement position sensor-less control for electronic commutation of the PMBLDC motor, which eliminates the need for mechanical Hall sensors and the related complex electric circuitry.

III. MAXIMUM POWER POINT TRACKING

Maximum Power Point Tracking (MPPT) is a useful tool in PV applications. The key factors that influence the electric power generated by a photovoltaic framework are solar radiation and temperature. The voltage at which a PV module can produce the maximum power is referred to as the "most extreme power point" (pinnacle control voltage). The fundamental rule of MPPT is in charge of isolating the most possible power from the solar and feeding it to the heap via a dc-to-dc converter that steps up/down the voltage to the desired size [5]. A PV generator's operational point is found at the junction of its current-voltage curve and the load-line. Its operating point may be distant from the generator's maximum power point (MPP), squandering a large portion of the available solar power. An MPP tracker, typically consisting of a basic dc-dc converter, is used to establish optimal matching between the PV generator and the load. An MPPT algorithm controls the duty ratio of the converter in order to optimise the power provided to the load.

A variety of MPPT algorithms, including the P&O algorithm, have been suggested [1-3]. This basic

technique, which is straightforward to construct, does not need prior knowledge of PV generator parameters or measurements of solar intensity and cell temperature. The method modifies the operating point by changing a control parameter by a tiny amount and then compares the PV array output power before and after the change. If the power grows, the algorithm continues to disrupt the system in the same direction; otherwise, the method perturbs the system in the opposite way.

The P&O technique is often implemented using two methods: reference voltage perturbation [4-10] and direct duty ratio perturbation [5, 7, 11-13]. The PV array output voltage reference is utilised as a control parameter in combination with a controller (often a PI controller) to adjust the duty ratio of the MPPT power converter for reference voltage perturbation. The PI controller gains are fine-tuned when the system is running at a constant voltage equal to the MPP voltage's standard test condition (STC). The MPPT algorithm controls the reference voltage while these gains remain constant. The duty ratio of the MPPT converter is employed directly as the control parameter for direct duty ratio perturbation.
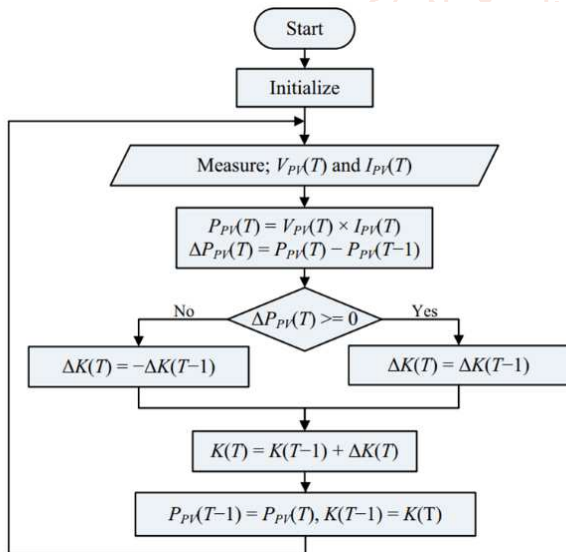

Fig 2: Flowchart of P&O MPPT algorithm

A. ZETA CONVERTER:

A zeta converter is a fourth order converter. Nonlinear system in the sense that it may be seen as a buck-boost-buck converter for energy input and a boost-buck-boost converter for output. The optimum switch-based zeta converter implementation is shown. Figure 3 depicts a non-isolated zeta converter circuit. While this converter may operate in a variety of modes depending on inductance value, load resistance, and operation frequency, only continuous inductor current " iL1" is examined here using the well-known state-space averaging approach. The following assumptions are used in the analysis.

- ➢ Semiconductors switching devices are regarded as ideal.
- ➢ The converter is in continuous inductor current mode.
- ➢ The line frequency ripple in the dc voltage is ignored.
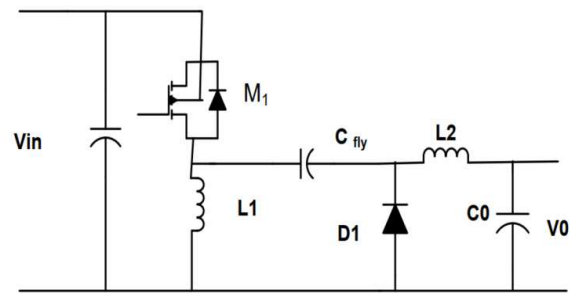
Fig 3: Proposed Structure of Basic Zeta converter

B. PRINCIPLE OF OPERATION:

When analysing Zeta converter, its waveform shows the equilibrium, L_1 average current equals I_{IN} and L_2 average current equals I_{out} since there is no DC current through the flying capacitor C_{FLY}. Also, there Stage-1[M_1ON]

The switch M1 is in ON state, so voltages VL_1 and VL_2 are equal to Vin . In this time interval diode D1 is OFF with a reverse voltage equal to - (V_{in} + V_o). Inductor L_1 and L_2 get energy from the voltage source, and their respective currents IL_1 and IL_2 are increased linearly by ratio V_{in}/L_1 and V_{in}/L_2 respectively. Consequently, the switch current IM1 = IL_1 + IL_2 is increased linearly by a ratio Vin/L, where L=$L_1.L_2/(L_1+L_2)$. At this moment, discharging of capacitor C fly and charging of capacitor C0 take place.
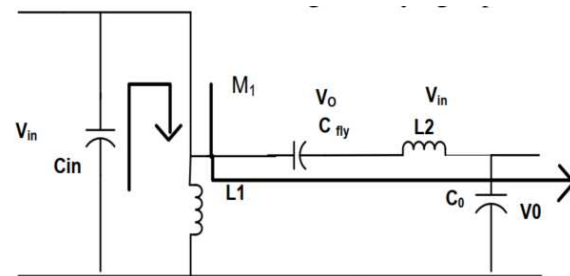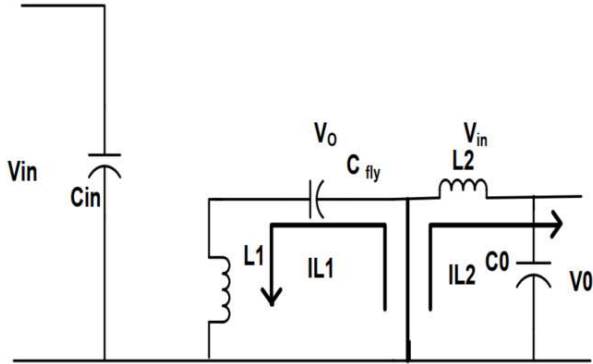

Fig 4: Zeta converter during MOSFET ON time

Stage-2 [M_1 OFF]

Is no DC voltage across either inductor. Therefore, C_{FLY} ground potential at its left side and V_{OUT} at its right side, resulting the DC voltage across C_{FLY} is equal to VOUT.

In this stage, the switch M_1 turns OFF and the diode D_1 is forward biased starting to conduct. The voltage

across L_1 and L_2 become equal to $-V_o$ and inductors L_1 and L_2 transfer energy to capacitor C_{fly} and load respectively. The current of L_1 and L_2 decreases linearly now by a ratio $-V_o/L1$ and $-V_o/L2$, respectively. The current in the diode $ID_1=IL_1+IL_2$ also decreases linearly by ratio $-V0/L$. At this moment, the voltage across switch M1 is $V_M = V_{in} + V_o$.

Fig 5: Zeta converter during MOSFET OFF time

DuVSI is used as a single-phase rectifier in PWM mode to charge the battery during ring regenerative braking. Table I shows the VSI switching procedure for both types of operation.

IV. CONTROL STRATEGY OF PROPOSED SYSTEM

The control of the proposed drive system is split into two parts: MPPT control in the front-end converter and load-end VSI control for optimum motor electronic commutation during driving and regenerative mode. In the preceding section, we discussed the MPPT control approach. As a result, the sensor-free electronic commutation approach of the PMBLDC motor with regenerative braking is thoroughly investigated here.

A. Electronic Commutation

The six-step electronic commutation of the PMBLDC motor is done by accurate switching of the VSI in 120-degree mode of operation using three virtual Hall sensor signals generated by the sensor less control algorithm. Two power switches are engaged at the same time on each 60-degree step. As a consequence, two phases of the motor are active at each commutation period, while the other phase remains quiet.

TABLE I. SWITCHING STATES OF THE VSI

Steps Mode	0°-60°	60°-120°	120°-180°	180°-240°	240°-300°	300°-360°
Motor	S1. S4	S1. S6	S3. S6	S3. S2	S5. S2	S5. S4
Regen.	S3. S2	S5. S2	S5. S4	S1. S4	S1. S6	S3. S6

B. Control Topology

The third harmonic stator flux is used here to allow electrical commutation of the motor without the need of a position sensor. The third harmonic flux is calculated using the motor's back emfs. The following is the Fourier series representation of the three phase back emfs:

$$e_A = E_1 sin\theta + E_1 sin3\theta + E_1 sin5\theta + \cdots \ldots (1)$$

$$e_B = E_1 sin(\theta - \frac{2\pi}{3}) + E_1 sin3(\theta - \frac{2\pi}{3}) + E_1 sin5(\theta - \frac{2\pi}{3}) + \cdots \ldots (2)$$

$$e_C = E_1 sin(\theta - \frac{4\pi}{3}) + E_1 sin3(\theta - \frac{4\pi}{3}) + E_1 sin5(\theta - \frac{4\pi}{3}) + \cdots \ldots (3)$$

Where θ is the electrical rotor angle. The sum of the three back-emf equations is expressed as,

$$e_A + e_B + e_C = 3E_3 sin3\theta + 3E_9 sin9\theta + E_{15} sin15\theta + \approx 3E_3 sin3\theta \quad (4)$$

Again, the total of the PMBLDC motor's three phase voltages is used,

$$u_{sum} = u_{an} + u_{bn} + u_{cn}$$

$$\left(Ri_A + L\frac{d}{dt}\right)(i_A + i_B + i_c) + (e_A + e_B + e_c)(5)$$

As in steady state, $(i_A + i_B + i_c) = 0,$

u_{sum} can be approximated as,

$$u_{sum} = e_A + e_B + e_c \approx 3E_3 sin 3\theta(6)$$

As a result of (4) and (6), it is possible to conclude that information about the third harmonic component of backemf is encoded in the sum of three phase voltages.

Now third harmonic stator flux can be obtained as,

$$\Psi_{3rd} = \int u_{sum} dt \, dt \quad (7)$$

As illustrated in Fig. 6, the generated third harmonic stator flux linkage from the integration of the u sum may be utilised to estimate the location of the rotor since the zero-crossing points of _3rd are the precise commutation points.
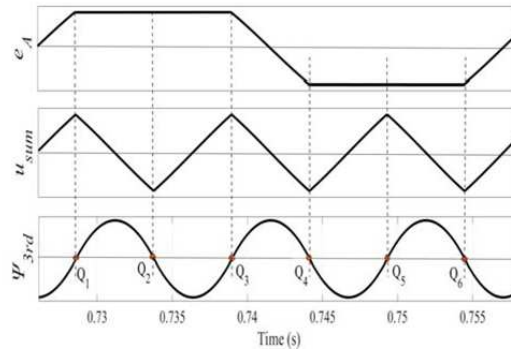
Fig 6: Relationship among back-emf and stator flux and zero-crossings

C. Elimination of false zero-crossings

The three back-emf signals are generated using the motor's terminal voltage. The observed terminal voltages in Fig. 7 exhibit unwanted spikes. This results in erroneous zero crossings and causes the VSI's whole switching logic to fail. A first order lowpass filter is designed to remove those annoying spikes.

The cut off frequency must be carefully chosen while creating the filter. Taking phase lag into account, the cut off frequency in this study is set at 1000 rad/s. The lowpass filter's transfer function is,

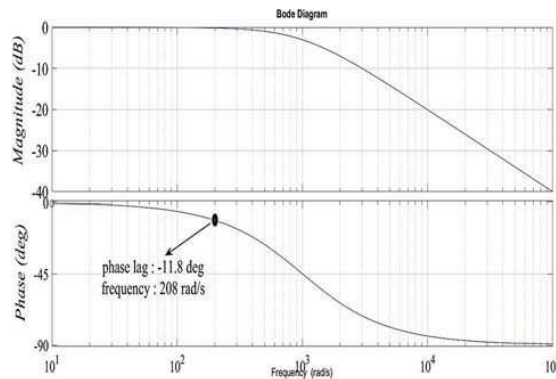$$H(s) = \frac{\omega_c}{s + \omega_c} = \frac{1000}{s + 1000} \quad (8)$$

The LPF adds some phase lag to the system. The phase lag in relation to the speed of the PMBLDC motor may be calculated as,

$$\phi = -\tan^{-1} \frac{\omega}{\omega_c} = -\tan^{-1}\left(\frac{2\pi \times 33.33}{1000}\right) = -11.7^o \quad (9)$$

Where the angular frequency of the derived back-emf is denoted by. The phase lag induced by the LPF while running at 1200 rpm is -11.7o, as illustrated in Fig 8.
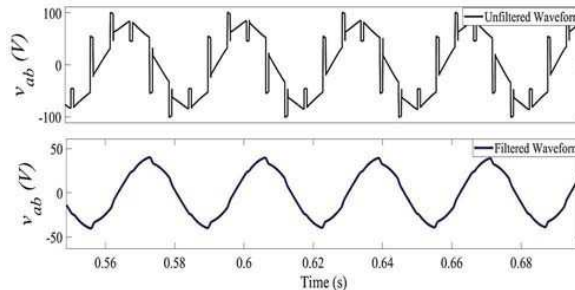
Fig 7: Unfiltered and filtered line voltage waveform

Fig 8: Bode plot diagram for lag compensator

D. Design Procedures of Lead Compensator

The phase lag generated by the lowpass filter causes mistakes in estimating the zero-crossing locations at greater speeds. Additionally, the torque ripple rises, potentially leading to considerable losses in the motor winding. As a consequence, to compensate for the additional lag, a compensator with a leading phase angle is necessary.

The lead compensator in this work is meant to correct for a phase lag of -11.8o at a frequency of 208.4 rad/s while the motor is operating at 1200 rpm. The compensator transfer function is expressed as follows,

$$G(s) = k\frac{s + \omega_{c1}}{s + \omega_{c2}} \quad (10)$$

Where k is the magnitude constant and c1 and c2 are the zero and pole crossover frequencies, respectively. The predicted value of k is,

$$k = \frac{1 + \sin\theta}{1 - \sin\theta} = \frac{1 + \sin 11.8}{1 - \sin 11.8} = 1.51 \quad (11)$$

The time constant T is,

$$T = \frac{1}{\omega \times \sqrt{k}} = \frac{1}{208.4 \times \sqrt{1.51}} = 3.90 \times 10^{-3} \, rad/s \quad (12)$$

So, the cut off frequencies are estimated as,

$$\omega_{c1} = \frac{1}{kT} = \frac{1}{1.51 \times 3.90 \times 10^{-3}} = 169.80 \, rad/s \quad (13)$$

$$\omega_{c1} = \frac{1}{kT} = \frac{1}{1.51 \times 3.90 \times 10^{-3}} = 256.41 \, rad/s \quad (14)$$

So, the transfer function becomes,

$$G(s) - k\frac{s + 169.80}{s + 256.41} \quad (15)$$

The Bode plot for the aforementioned system is shown in Fig. 9. At frequency 208 rad/s, a phase lead of 11.8o is effectively achieved. Figure 7 shows the filtered waveform of the terminal voltage, which has been filtered to remove any undesired spikes. With these filtered and rectified waveforms, the commutation error of the PMBLDC motor may be considerably decreased.
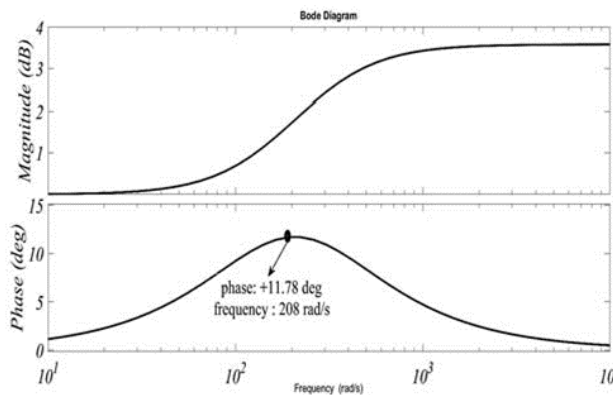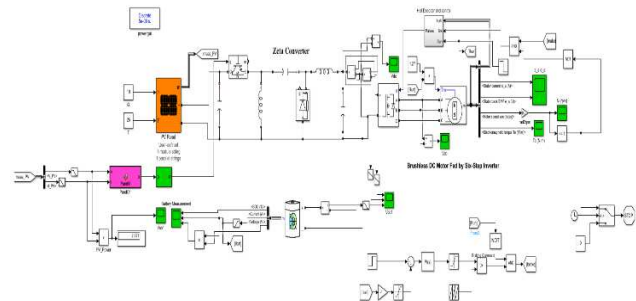

Fig 9: Bode plot diagram for lead compensator

V. RESULTS AND DISCUSSION SIMULATION AND RESULTS

The complete EV model is simulated in MATLAB, the detailed simulation results along with discussions as follows.

➢ Performance of solar PV array
➢ Performance of Zeta Converter
➢ Performance of PMBLDC motor

Fig 10: Simulink Model of the PV battery fed EV system with regenerative braking employing zeta converter

To analyse the performance of the solar PV battery fed ev system with regenerative braking employing zeta converter. The PV parameters of the system are shown in Table II.

TABLE II: PV PARAMETERS

Parameters	Specifications
Maximum power (W)	334.905 W
Parallel strings	1
Series-connected modules per string	1
Cells per module (Ncell)	80
Open circuit voltage Voc (V)	49.9
Short-circuit current Isc (A)	9
Voltage at maximum power point Vmp (V)	41.5
Current at maximum power point Imp (A)	8.07

Performance evaluation of a solar PV battery-fed electric vehicle with regenerative braking using a zeta converter at 1000 IR and 25 Degree Temp, Solar (PV) and Battery Both the source are used while testing the proposed system.

Figures 12, 15, 20 and 23 show results for regenerative braking at 0.5 sec; when braking was applied, torque and speed went negative, and the battery started charging via regenerative braking.
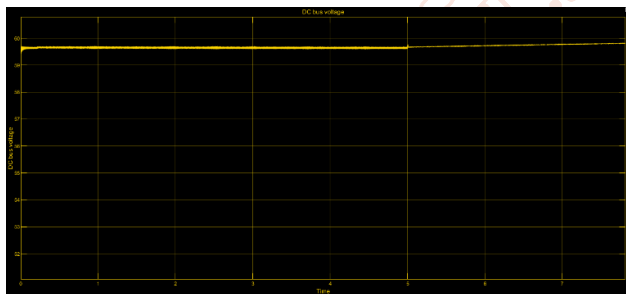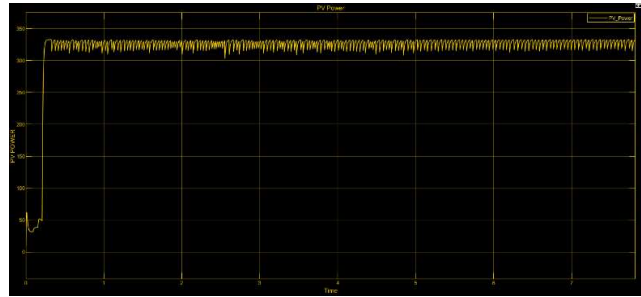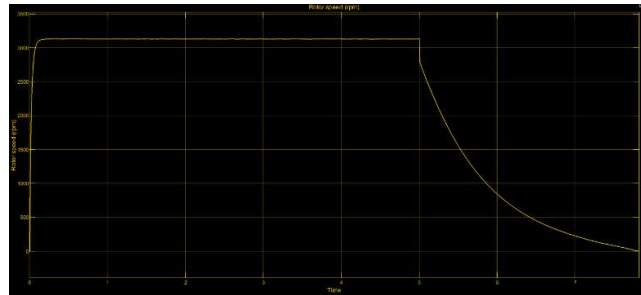

Fig 11: DC Bus Voltage Vs Time in (S)
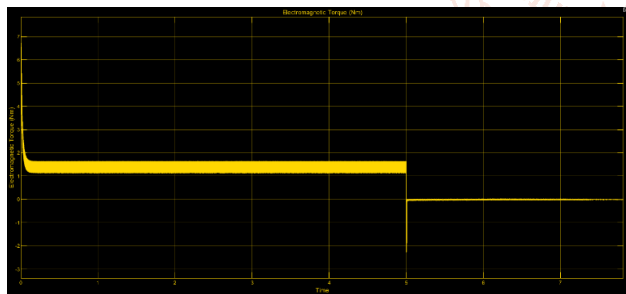
Fig 12: Electromagnetic Torque (NM) of BLDC Motor Vs Time in (S)
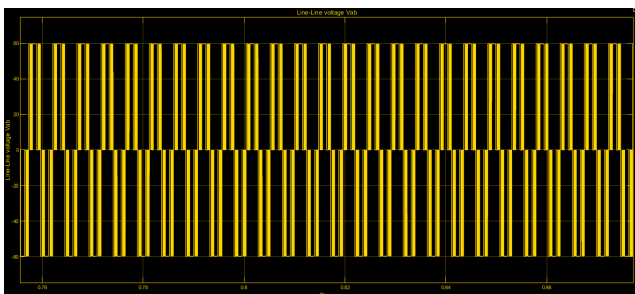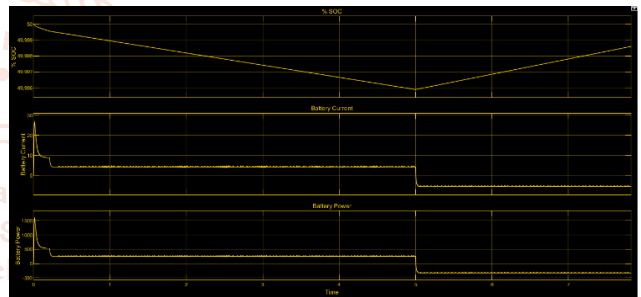

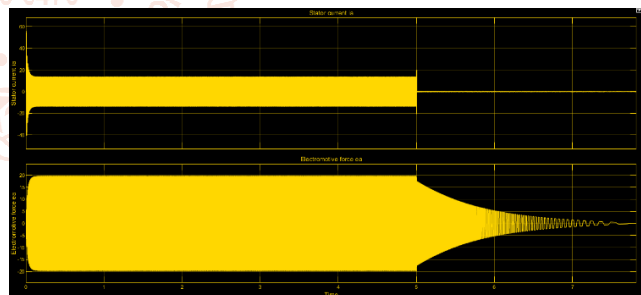**Fig 13: Line – Line Voltage (Vab) Vs Time in (S)**

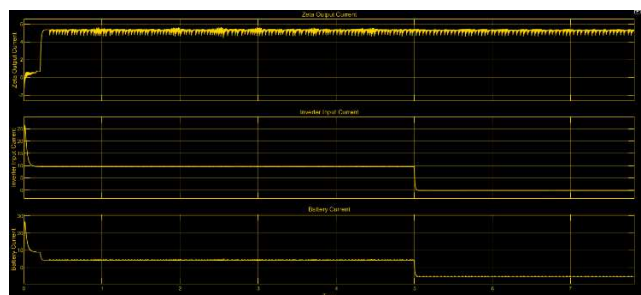
Figure 14. PV Power Vs Time in (S)

Fig 15: Rotor Speed (RPM) of BLDC Motor Vs Time in (S)

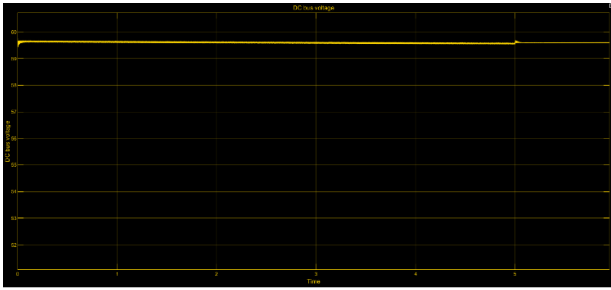**Fig 16: SOC %, Battery Current and Battery Power Vs Time in (S)**

Fig 17: Stator Current Ia and Electromotive Force Ea Vs Time in (S)
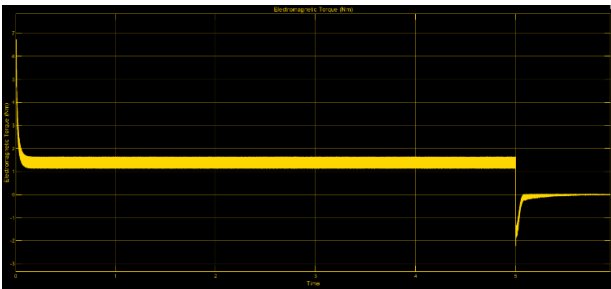

Fig 18: Zeta Converter Output Current, Inverter Input Current and Battery Current Vs Time in (S)
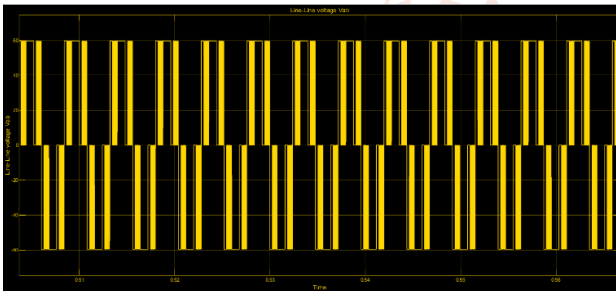
Performance evaluation of a solar PV battery-fed electric vehicle with regenerative braking using a zeta converter at 10 IR and 25 Degree Temp, PV power is zero, so battery power is the only source used while testing the proposed system.
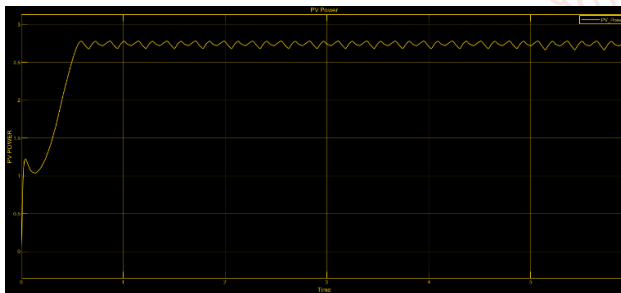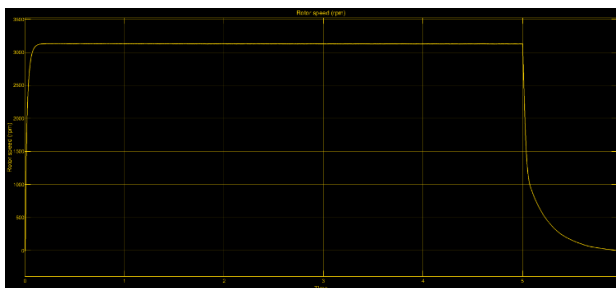

Fig 19: DC Bus Voltage Vs Time in (S)

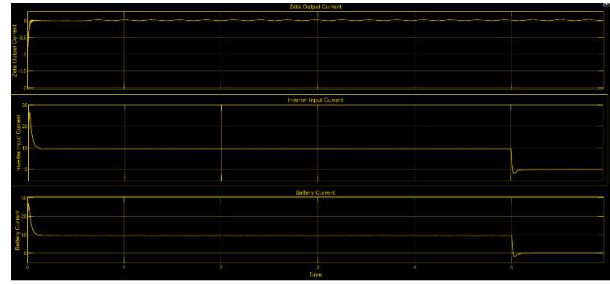Fig 20: Electromagnetic Torque (NM) of BLDC Motor Vs Time in (S)

Fig 21: Line – Line Voltage (Vab) Vs Time in (S)
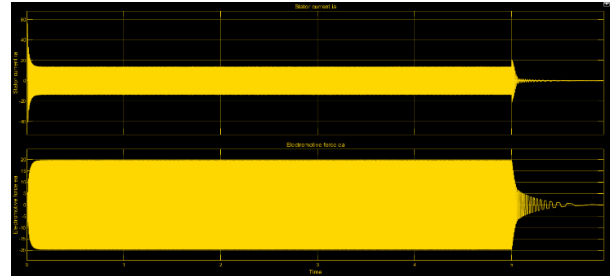

Fig 22: PV Power Vs Time in (S)
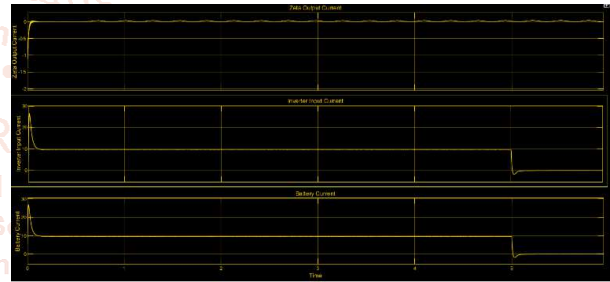

Fig 23: Rotor Speed (RPM) of BLDC Motor Vs Time in (S)

Fig 24: SOC %, Battery Current and Battery Power Vs Time in (S)

Fig 25: Stator Current Ia and Electromotive Force Ea Vs Time in (S)

Fig 26: Zeta Converter Output Current, Inverter Input Current and Battery Current Vs Time in (S)

VI. CONCLUSION

This paper describes an electric vehicle power train with regenerative braking technology and speed control of a PMBLDC motor driven by a solar-PV and battery system. The speed is managed online based on the peak power of the solar-PV panel and the load requirement. The battery is charged by the vehicle's kinetic energy during braking, allowing regeneration to occur. The intermediary DC-DC converter step is removed during this operation. A noninverted zeta converter with constant output current provides effective MPPT control of a solar-PV array. The VSI switches are gated at fundamental frequency, which reduces the losses associated from high-frequency switching. In terms of stability and controllability, the developed system is supposed to be robust.

REFERENCES

[1] Valentin Totev; Vultchan Gueorgiev "Efficiency of Regenerative Braking in Electric Vehicles" 2020 21st International Symposium on Electrical Apparatus & Technologies (SIELA).

[2] Abhishek Gaurav; Anurag Gaur "Modelling of Hybrid Electric Vehicle Charger and Study the Simulation Results" 2020 International Conference on Emerging Frontiers in Electrical and Electronic Technologies (ICEFEET).

[3] Dragos Niculae; Mihai Iordache; Marilena Stanculescu; Maria Lavinia Bobaru; Sorin Deleanu "A Review of Electric Vehicles Charging Technologies Stationary and Dynamic" 2019 11th International Symposium on Advanced Topics in Electrical Engineering (ATEE).

[4] Ahad Javandoust Qarebagh; Farnaz Sabahi; Dariush "NazarpourOptimized Scheduling for Solving Position Allocation Problem in Electric Vehicle Charging Stations" 2019 27th Iranian Conference on Electrical Engineering (ICEE).

[5] Junbeom Wi; Hyunhwa Kim; Jiho Yoo; Hanho Son; Hyunsoo Kim; Byungjae Kim "Energy consumption of parallel type hybrid electric vehicle with continuously variable transmission using electric oil pump" 2018 Thirteenth International Conference on Ecological Vehicles and Renewable Energies (EVER).

[6] Chaoqun Liu; Bin Wei; Songcen Wang; Xiaokang Wu; Xian Zhang; Jie Wang; Qingxin Yang "Field Circuit Coupling Analysis of Dynamic Wireless Charging for Electric Vehicle" 2018 IEEE 2nd International Electrical and Energy Conference (CIEEC).

[7] Jing Zhang; Hui Yan; Ning Ding; Jian Zhang; Taoyong Li; Shu Su "Electric Vehicle Charging Network Development Characteristics and Policy Suggestions" 2018 International Symposium on Computer, Consumer and Control (IS3C).

[8] Araz Saleki; Saman Rezazade; Mahmudreza Changizian "Analysis and simulation of hybrid electric vehicles for sedan vehicle" 2017 Iranian Conference on Electrical Engineering (ICEE).

[9] V. P. Dhote; M. M. Lokhande; Akash Agrawal; B. Hemanth Kumar "Mechanical coupling of two induction motor drives for the applications of an electric-drive vehicle system" 2017 National Power Electronics Conference (NPEC).

[10] Oliver Marcincin; Zdenek Medvec; Petr Moldrik "The impact of electric vehicles on distribution network" 2017 18th International Scientific Conference on Electric Power Engineering (EPE).

[11] Fatemeh Jozi; Kazem Mazlumi; Hadi Hosseini "Charging and discharging coordination of electric vehicles in a parking lot considering the limitation of power exchange with the distribution system" 2017 IEEE 4th International Conference on Knowledge-Based Engineering and Innovation (KBEI).

[12] Egor Kulik; Xuan Trung Tran; Alecksey Anuchin; Yuriy Vagapov "GPS-track data processing for the optimization of the powertrain for hybrid electric vehicles" 2017 IEEE 58th International Scientific Conference on Power and Electrical Engineering of Riga Technical University (RTUCON).

[13] Somayyeh Khatiri-Doost; Meysam Amirahmadi "Peak shaving and power losses minimization by coordination of plug-in electric vehicles charging and discharging in smart grids" 2017 IEEE International Conference on Environment and Electrical Engineering and 2017 IEEE Industrial and Commercial Power Systems Europe (EEEIC / I&CPS Europe).

[14] X. D. Xue; K. W. E. Cheng; S Raghu Raman; Jones Chan; J. Mei; C. D. Xu "Performance prediction of light electric vehicles powered by body-integrated super-capacitors" 2016 International Conference on Electrical Systems for Aircraft, Railway, Ship Propulsion and Road Vehicles & International Transportation Electrification Conference (ESARS-ITEC).

[15] Muhammad Sifatul Alam Chowdhury; Khandakar Abdulla Al Mamun; Al Mahmudur Rahman" Modelling and simulation of power system of battery, solar and fuel cell powered Hybrid Electric vehicle" 2016 3rd International Conference on Electrical Engineering and Information Communication Technology (ICEEICT).